Effects of composition on the structure, thermal and some physical characteristics of Bi_2O_3-B_2O_3-ZnO-SiO_2 glasses

Yu. S. Hordieiev*, A. V. Zaichuk
Ukrainian State University of Chemical Technology, 8 Gagarin Avenue, Dnipro, 49005, Ukraine

The influence of composition on the structure, thermal, and some physical characteristics of bismuth borate glasses, formulated as $55Bi_2O_3$–$(35-x-y)B_2O_3$–$(5+x)$ZnO–$(5+y)SiO_2$ (where $0 \leq x, y \leq 15$ mol%), was investigated. Comprehensive analyses were conducted using techniques such as X-ray Diffraction (XRD), Scanning Electron Microscopy (SEM), Fourier-Transform Infrared Spectroscopy (FTIR), Differential Thermal Analysis (DTA), and Dilatometry. XRD confirmed the amorphous nature of the glass samples, while FTIR spectroscopy revealed that the glasses are primarily composed of BO_4, BO_3, BiO_6, BiO_3, ZnO_4, and SiO_4 structural units. DTA provided further evidence of the samples' glassy state and insights into key temperatures like glass transition (T_g), crystallization (T_c), and melting (T_m). The study finds that substituting B_2O_3 with SiO_2 increases all characteristic temperatures, whereas replacing it with ZnO decreases T_g and T_c but increases T_m. The maximum thermal stability, indicated by a ΔT of 99°C, was observed in the glass with a $55Bi_2O_3$–$20B_2O_3$–20ZnO–$5SiO_2$ composition. Dilatometric measurements showed that the investigated glasses have a high coefficient of thermal expansion (10.0–10.7 ppm/°C) values, a low glass transition temperature (345–376°C), and a low dilatometric softening temperature (364–392°C). Additionally, the density and molar volume of the samples were accurately determined.

(Received February 5, 2024; Accepted May 3, 2024)

Keywords: Glasses, Glass transition, Thermal expansion, Glass stability, Density

1. Introduction

Bismuth zinc borosilicate glasses stand as a groundbreaking advancement within the domain of heavy metal oxide glasses, characterized by their exceptional qualities such as elevated refractive indices, reduced softening points, high density, and superior nonlinear optical susceptibilities [1–3]. These attributes herald these glasses as a pivotal subject in the field of materials science, especially since they offer promising applications in the development of cutting-edge optical devices and effective radiation shielding solutions [4, 5]. The composition of these glasses involves a harmonious blend of bismuth oxide, boron oxide, silicon dioxide, and zinc oxide, with each component playing a pivotal role in defining the glasses' overall performance and suitability for various uses. One of the key components, bismuth oxide, though not a conventional network former due to the low field strength of the bismuth ion [6], forms a stable glass network when combined with B_2O_3 and SiO_2 [7]. This synergy allows for a broad compositional range and enhances the material's structural stability. The presence of zinc oxide further augments these properties, contributing to lower melting temperatures and improving the glass's chemical durability [8, 9]. One of the most remarkable aspects of bismuth zinc borosilicate glasses is their application in photonic and optoelectronic devices [10]. Their high nonlinear optical properties make them ideal for use in optical switches, broadband amplifiers, and waveguides [11]. Additionally, their high refractive index and transparency across a broad spectrum make them suitable for advanced optical components. Furthermore, these glasses exhibit excellent thermal stability and chemical durability, qualities that are essential for long-term applications in harsh

* Corresponding author: yuriihordieiev@gmail.com
https://doi.org/10.15251/JOR.2024.203.273

environments [12]. Their low melting points and ease of fabrication also make them attractive from a manufacturing perspective.

Bismuth zinc borosilicate glasses are environmentally friendly due to their use of bismuth oxide instead of lead oxide [13], which has historically been a common component in many glass formulas despite its significant health and environmental drawbacks. The shift towards bismuth oxide reflects growing ecological concerns and stricter regulations, making these glasses a safer and more eco-friendly choice for various applications.

Although bismuth zinc borosilicate glasses have clear advantages, their full capabilities are still being explored. Contemporary research focuses on unraveling the intricate relationships among the glasses' chemical composition, atomic structure, and resulting characteristics. This deep dive into their intrinsic characteristics aims to unlock and enhance their suitability for a wide array of applications, pushing the boundaries of their utility.

To that end, this study has been carefully designed to examine how variations in composition affect the glasses' structural, thermal, and physical characteristics, especially for those with a high concentration of bismuth oxide. The ultimate goal is to unlock a deeper understanding of bismuth zinc borosilicate glasses, paving the way for their optimized application across various domains, thereby developing safer, more sustainable, and environmentally friendly glass alternatives.

2. Materials and methods

Table 1 presents the compositions and labels of the glasses under study. In the course of this study, we employed the conventional melt quench process to fabricate glasses within the compositional range of $55Bi_2O_3$–$(35-x-y)B_2O_3$–$(5+x)ZnO$–$(5+y)SiO_2$, where the concentrations of ZnO and SiO2 were adjusted within the range of 0 to 15 mol%. The synthesis process harnessed exceptionally pure starting materials: Bismuth Oxide (Bi_2O_3) at 99.9% purity sourced from Sigma–Aldrich, Boric Acid (H_3BO_3) at 99.9% purity from Eti Mine Works, Zinc Oxide (ZnO) at 99.7% purity from Reachim, and Silicon Dioxide (SiO_2) at 99.96% purity provided by Polar Quartz. These materials underwent a rigorous mixing process to achieve a homogeneous blend before being subjected to the melting process. Melting was performed using a high-quality platinum (Pt) crucible in an electric furnace. This furnace was equipped with silicon carbide (SiC) heating elements to provide a stable and uniform heating environment. The furnace temperature was set at 1050°C, and materials were melted for 45 minutes to ensure homogeneity. After melting, the molten glass was immediately poured into a stainless steel mold for shaping [14]. The glass was then subjected to a controlled annealing process to minimize the development of internal stresses and improve the structural integrity of the glass [15]. This involved placing the glass in a muffle furnace set at 360°C for a period of 5 hours to allow for slow and uniform cooling.

Table 1. The chemical composition (in mol%) and the sample codes of the glasses that have been studied.

Sample code	Bi_2O_3	B_2O_3	ZnO	SiO_2
35B5Z5S	55	35	5	5
30B10Z5S	55	30	10	5
25B15Z5S	55	25	15	5
20B20Z5S	55	20	20	5
30B5Z10S	55	30	5	10
25B10Z10S	55	25	10	10
20B15Z10S	55	20	15	10
25B5Z15S	55	25	5	15
20B10Z15S	55	20	10	15
20B5Z20S	55	20	5	20

In order to perform Differential Thermal Analysis (DTA) on glass samples, the first step was to convert each sample to a finely ground powder with extreme care. An agate mortar and pestle were used to ensure a consistent particle size throughout the grinding process. The finely ground powder was subsequently subjected to a sieving process. Specifically, the particles that successfully passed through a 270-mesh (53μm) sieve were collected for further DTA examination [14–16]. Differential Thermal Analysis was performed using a Derivatograf Q-1500D, which uses Pt crucibles to withstand the high temperatures involved in the analysis [17]. This setup enabled the precise measurement of thermal properties by comparing the sample's behavior to that of a high-purity alumina reference material. The analysis protocol involved controlled heating of the samples alongside the reference at a steady rate of 5°C per minute within an atmospheric air environment. This process spanned a temperature range extending from ambient conditions up to 1000°C. The analysis focused on identifying key characteristic temperatures that are crucial for understanding the thermal behavior and stability of the glass materials [13, 18]. These temperatures included the glass transition temperature (T_g), which marked the onset of softening in the glass and was identified at the point where the first endothermic deviation occurs on the DTA curve [17–20]. Additionally, the onset of crystallization temperature (T_x) was determined at the beginning of the exothermic deviation, indicating the start of crystalline phase formation. The peak temperature (T_c) of crystallization was identified as the apex of the exothermic peak, highlighting the point of most intense crystallization activity [13, 18]. Subsequent studies aimed at detecting the presence of crystalline phases after the thermal treatment, which involved keeping the glass powder at the T_c in an air atmosphere for five hours [15, 16]. X-ray diffraction analysis using a DRON-3M instrument with Co-Kα radiation (1.79026 Å) confirmed the appearance of crystalline phases. In addition, the structural features of these crystalline formations were studied by scanning electron microscopy using a Tescan MIRA3 instrument, providing insight into their morphology.

The study also utilized Fourier-transform infrared spectroscopy to obtain transmitting spectra of the samples, using a Thermo-Nicolet Avatar 370 FT-IR Spectrometer in the 1400–400 cm^{-1} range, with a 2 cm^{-1} resolution [14–16]. For this, glass powder was blended with potassium bromide (KBr) in a 2:200 ratio and compressed into 13 mm diameter pellets [19]. The resulting spectra averaged over 32 scans against a KBr baseline [15, 16], providing precise analysis.

Additionally, essential thermal attributes, including the dilatometric softening point (T_d), glass transition temperature (T_g), and the coefficient of thermal expansion (CTE) [14–16], were determined with high precision. These measurements were facilitated by a DILA GT-1300 dilatometer, which operated at a heating rate of 3°C/min, assessing the CTE across a 20 to 300°C temperature range [16]. The glass density, a critical parameter, was measured at ambient conditions employing the Archimedes principle with distilled water [16, 18], ensuring accuracy through multiple trials and maintaining a maximum uncertainty margin between 0.006–0.014 g/cm^3.

3. Results and discussion

Figure 1 showcases the XRD patterns for the newly synthesized glass samples across a 2Θ angle span from 10 to 90 degrees. The patterns do not exhibit the expected sharp peaks of crystalline substances but instead display a broad hump within the 25° to 40° range. This feature indicates that the glass samples are amorphous, i.e., they have no long-range atomic order. The presence of this broad hump highlights the existence of some degree of short-range order amidst an overall disordered structure. This observation underscores the fundamental distinction between amorphous materials, such as the glass samples in this study, and crystalline materials, which exhibit well-defined, sharp diffraction peaks due to their highly ordered atomic structures.

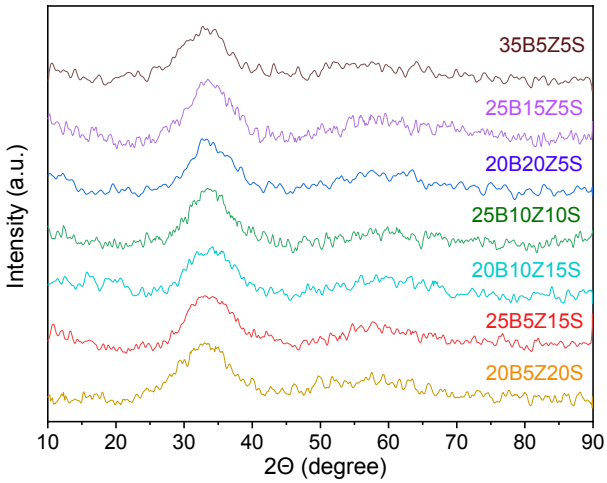

Fig. 1. XRD results of the fabricated $55Bi_2O_3$-$(35-x-y)B_2O_3$-$(5+x)ZnO$-$(5+y)SiO_2$ glass samples.

Fourier-transform infrared (FT-IR) spectroscopy serves as an invaluable method for exploring how variations in glass composition impact its local structural units. This is clearly illustrated by the FT-IR spectra of four different glass samples: 35B5Z5S, 25B10Z10S, 20B5Z20S, and 20B20Z5S. Figure 2 showcases these spectra, captured in the 1400 to 400 cm^{-1} frequency range, providing a detailed comparison of their structural characteristics. Notably, the FTIR spectra of these samples are marked by five distinct groups of absorption bands. One of the most pronounced features is a broad absorption band with dual peaks spanning the 1350–1100 cm^{-1} range. This band, along with others located at approximate frequencies of 1018, 890, 700, and 470 cm^{-1}, delineates significant structural characteristics of the glass samples under study. Specifically, the band near 1250 cm^{-1} is associated with the asymmetric stretching vibrations of borate (B–O and B–Ø) bonds present in BO_3 and $BO_2Ø$ units, where "Ø" signifies a non-bridging oxygen atom [15, 20–23]. A discernible band in the vicinity of 1190–1164 cm^{-1}, which gains prominence as B_2O_3 is substituted by ZnO, correlates to the stretching vibrations of B–O bonds in BO_3 units associated with meta, pyro, and orthoborate configurations [15, 16, 23]. Meanwhile, the band around ~1018 cm^{-1}, associated with B–O stretching vibrations in BO_4 units from various borate groups, exhibits a diminishing intensity as the content of SiO_2 and ZnO increases, suggesting alterations in the borate network structure with compositional changes [16, 24]. The conspicuous band at approximately 890 cm^{-1} is attributed to the symmetric stretching vibration of Bi–O in BiO_3 pyramidal units and the asymmetric vibrations of Si–O–Si in SiO_4 tetrahedra, as documented in references [4, 25]. The band centered at 706–700 cm^{-1} is associated [16, 26] with the B–O–B bending vibration in BO_3 triangles, with its intensity and spectral area expanding upon the equimolar substitution of B_2O_3 with ZnO, suggesting an augmentation in BO_3 units, while a concurrent decrease in the band at 1020 cm^{-1} signals a diminution in BO_4 structures. The last noted absorption band, centered approximately at 480 cm^{-1}, is linked to the bending vibration of the Bi–O bond in highly distorted BiO_6 units and the Zn–O bond in ZnO_4 units [16, 18, 27]. This comprehensive analysis underscores the profound impact of glass composition on its structural characteristics, as revealed through FT-IR spectroscopy, advancing our understanding of the structural dynamics at play in these materials.

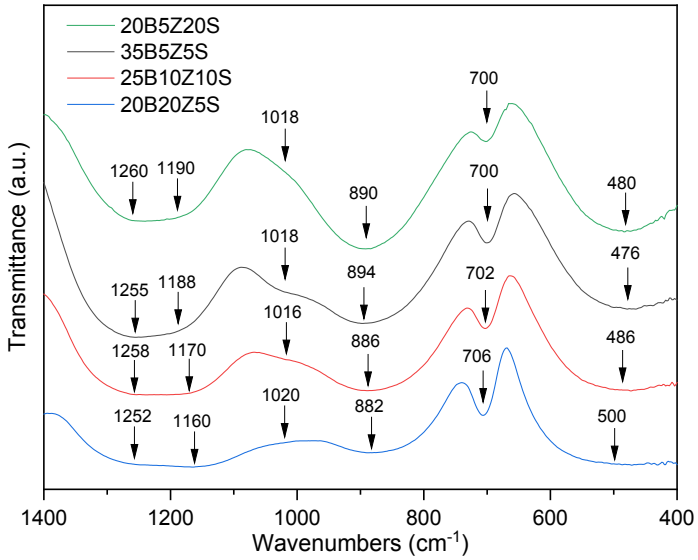

Fig. 2. FT-IR results of selected bismuth zinc borosilicate samples.

Studying glasses' thermal and crystallization behavior is critical to understanding their inherent properties and exploring their potential applications. Differential Thermal Analysis is a key methodology for assessing thermal behaviors in various materials, especially glasses [16]. Figure 3 illustrates the DTA plots for the studied bismuth zinc borosilicate glasses, providing a comprehensive view of key characteristic temperatures [16, 28]. In addition, Table 2 lists the characteristic temperatures derived directly from the DTA analysis. This data is indispensable for researchers and engineers, facilitating the advancement of glass science and the development of new glass-based applications.

Table 2. Density, molar volume and thermal characteristics of $55Bi_2O_3$-$(35-x-y)B_2O_3$-$(5+x)ZnO$-$(5+y)SiO_2$ glasses.

Glass sample code	Density, (g/cm^3)	Molar volume, (cm^3/mol)	DTA				Stability parameters			
			T_g, °C	T_x, °C	T_c, °C	T_m, °C	ΔT, °C	K_{SP}	K_H	T_{gr}
35B5Z5S	7.264	39.61	369	448	464	645	79	3.43	0.52	0.57
30B10Z5S	7.365	39.14	355	439	454	654	84	3.55	0.50	0.54
25B15Z5S	7.477	38.64	350	442	456	662	92	3.68	0.51	0.53
20B20Z5S	7.565	38.27	346	445	462	677	99	4.86	0.54	0.51
30B5Z10S	7.299	39.35	370	452	470	647	82	3.99	0.56	0.57
25B10Z10S	7.406	38.86	366	450	466	656	84	3.67	0.53	0.56
20B15Z10S	7.496	38.48	356	451	468	680	95	4.54	0.53	0.52
25B5Z15S	7.318	39.19	372	452	472	647	80	4.30	0.57	0.57
20B10Z15S	7.425	38.70	364	444	470	674	80	5.71	0.52	0.54
20B5Z20S	7.333	39.04	374	454	475	650	80	4.49	0.58	0.58

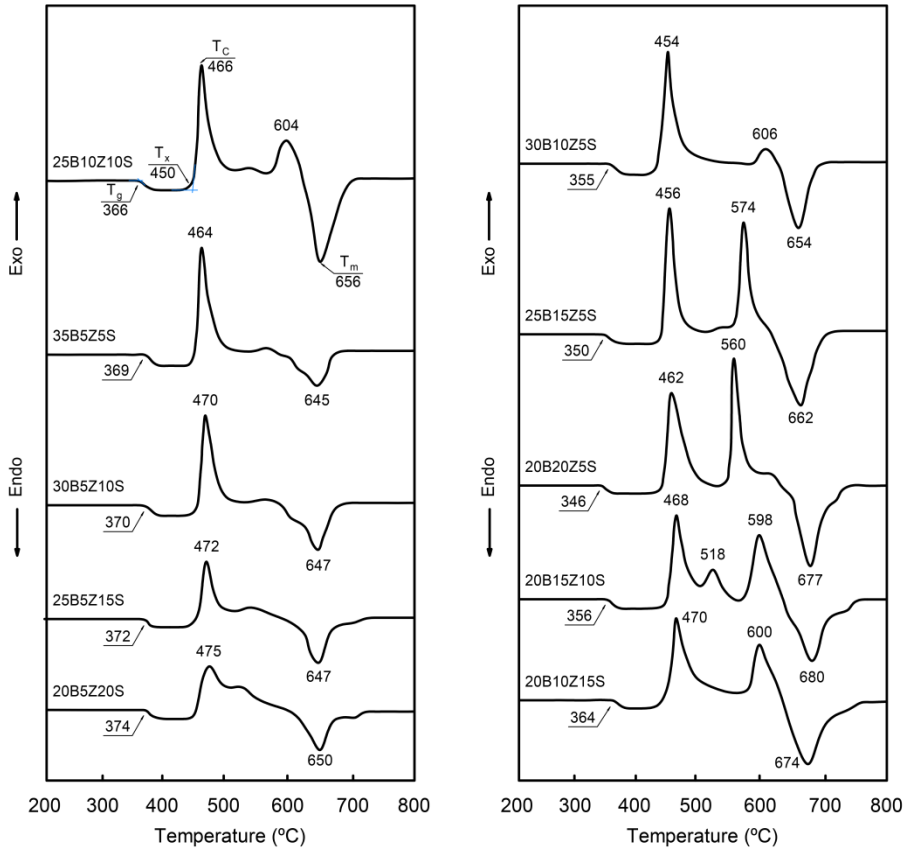

Fig. 3. DTA results of $55Bi_2O_3$–$(35-x-y)B_2O_3$–$(5+x)ZnO$–$(5+y)SiO_2$ glasses.

The research indicates that replacing B_2O_3 with SiO_2 in the glass composition elevates all characteristic temperatures. Conversely, substituting B_2O_3 with ZnO results in a decrease in the glass transition and crystallization temperatures while the melting temperature increases. The detection of an endothermic shift within the 345 to 380°C range across all DTA scans underscores the occurrence of a glass transition, corroborating the amorphous nature of the glass samples under investigation [18]. The glass transition temperature varies with changes in chemical composition, decreasing from 369 to 346°C as ZnO content increases and increasing from 369 to 375°C as SiO_2 content increases. The rationale behind the decline in T_g with higher ZnO content, substituting for B_2O_3, lies in the comparatively weaker bond energy of Zn–O (151 kJ/mol) versus that of B–O (372 kJ/mol) [29]. In contrast, substituting B_2O_3 with SiO_2 elevates T_g values owing to the stronger Si–O bond strength (443 kJ/mol) relative to B–O bonds.

Furthermore, glass compositions incorporating zinc oxide at concentrations of 10 mol% or above display two exothermic peaks during DTA analysis, illustrating intricate crystallization dynamics and the emergence of two separate crystalline phases. Conversely, an increase in silicon dioxide content is correlated with a decrease in the intensity of these exothermic peaks, suggesting that higher SiO_2 concentrations may inhibit the crystallization process, contributing to the glass's thermal stability and amorphous nature.

For further analysis, the glass powders were heat treated for five hours at their respective T_c, and phase identification was performed via powder diffraction file (PDF) analysis [15, 16]. The study's DTA analysis indicated varying T_c for different compositions: 464°C for 35B5Z5S, 475°C for 20B5Z20S and two temperatures, 462°C and 560°C, for 20B20Z5S. Figure 4 shows the X-ray diffraction results for each sample after heat treatment at the specified temperatures. XRD analysis revealed that a single crystalline phase, $Bi_4B_2O_9$ (PDF 01-070-1458), was formed by heating the base glass (35B5Z5S) at 464℃ for five hours. The 20B5Z20S sample, post-heat treatment, exhibited two phases: $Bi_4B_2O_9$ and Bi_2SiO_5 (00-036-0287). The 20B20Z5S composition exhibited distinct phases across different temperatures: at 462°C, the phases of $Bi_4B_2O_9$ and $Bi_{12}ZnO_{20}$ (PDF

01-078-1325) were observed, while heating at 560°C resulted in the phase of $Bi_4ZnB_2O_{10}$ (PDF 00-041-0701). To complement these findings, Figure 5 shows SEM micrographs of the fractured surfaces of these glass-ceramic samples, providing a closer look at the microstructural changes. As shown in Fig. 5, the 35B5Z5S sample exhibited a unique fibrous crystal morphology with needle-like features. The crystals are tightly packed together, exhibiting a sort of woven texture. A sample containing 20 mol% SiO_2 (20B5Z20S) showed a more heterogeneous surface with different and larger crystal formations interspersed with an amorphous phase, suggesting that the increased SiO_2 content leads to different crystal shapes and sizes. The 20B20Z5S sample with high ZnO content displays a dendritic growth pattern resembling tree-like branches. The crystals in this sample have a high aspect ratio, with long, thin primary branches and numerous secondary offshoots.

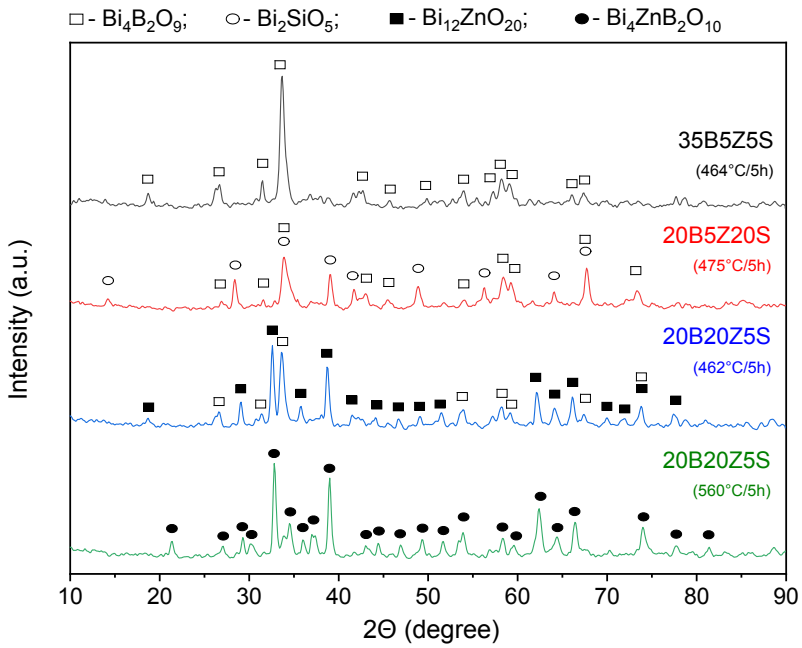

Fig. 4. XRD findings of glass powders subjected to heat treatment at their respective peak crystallization temperatures.

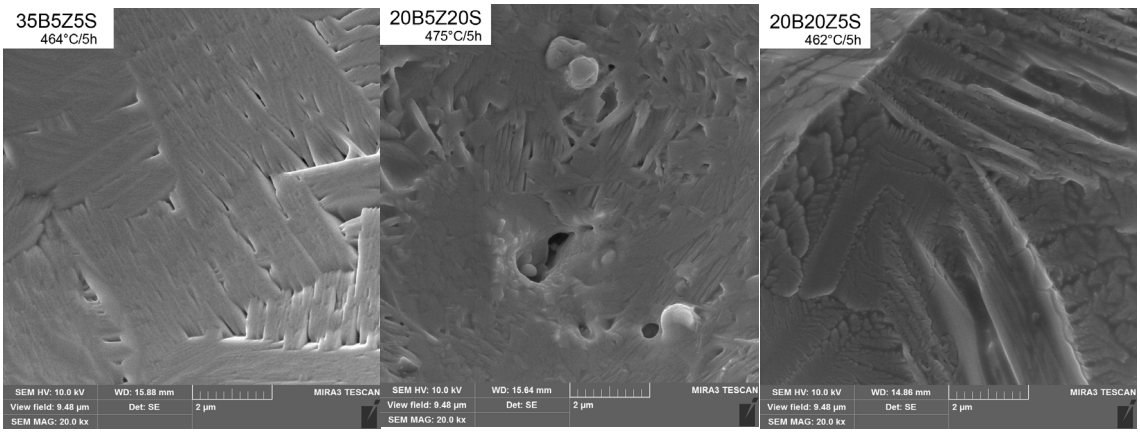

Fig. 5. SEM image of the fracture surfaces of 35B5Z5S, 20B5Z20S, and 20B20Z5S samples following a 5-hour heat treatment.

Glass forming ability (GFA) and glass stability (GS) are important characteristics that determine the behavior of glass materials during cooling and heating processes [30, 31]. GFA refers to the resistance to crystallization when a glass melt is cooled [30], while GS is the resistance to crystallization when glass is heated [31]. Various parameters based on characteristic temperatures (like T_g, T_x, T_c, and T_m) are used to evaluate these properties. A key parameter for assessing thermal stability is the Dietzel criterion [32], represented as $\Delta T = T_x - T_g$. A larger ΔT value indicates higher thermal stability of the glass, suggesting a wider sintering window. Enhancements in thermal stability are noted with the equimolar substitution of B_2O_3 by ZnO and SiO_2 in the base glass composition, as evidenced by an increase in ΔT from 79 to 99°C. Another valuable metric for understanding glass stability is the parameter proposed by Saad and Poulain [33], expressed as $K_{SP} = ((T_c - T_x)\Delta T)/T_g$. This parameter provides insight into the thermal stability and resistance to the devitrification of glass. Higher K_{SP} values indicate improved stability and the compositional changes mentioned earlier also increase K_{SP} values, further confirming the enhanced thermal stability. Hruby's parameter [34], defined as $K_H = (T_c - T_g)/(T_m - T_c)$, sheds light on the ease of glass formation. Hruby's theory posits that higher K_H values suggest a glass's greater resistance to crystallization during heating and a stronger ability to preserve its amorphous state during cooling [16]. Forming glasses with $K_H \leq 0.1$ is challenging and requires rapid cooling, whereas glasses with $K_H \geq 0.5$ are more easily formed at moderate quenching rates. The studied glasses show K_H values between 0.50 and 0.58, denoting excellent glass-forming ability and high resistance to crystallization. Another widely used indicator, the reduced glass transition temperature (defined as $T_{rg} = T_g/T_m$) [35], aids in estimating GFA. The T_{rg} values obtained in this study, which range from 0.51 to 0.58, comply with the Kauzmann criteria ($0.5 \leq T_{rg} \leq 0.66$) [36], indicating that the studied glass compositions have good glass-forming capabilities.

Dilatometry is an essential technique for gaining insights into the thermal characteristics of glass, playing a pivotal role in evaluating its appropriateness for various uses [37]. The dilatometry curve (Fig. 6a), a key output of this process, reveals three crucial properties: it's coefficient of thermal expansion (CTE), the glass transition temperature (T_g), and the dilatometric softening temperature (T_d) [16]. The glass's oxide composition significantly affects these properties. Thus, comprehending how oxide composition impacts the glass's thermal properties is crucial for customizing glass formulations for specific needs.

Figures 6b-d illustrate the influence of compositional variations on fundamental thermal properties within the $55Bi_2O_3$–$(35-x-y)B_2O_3$–$(5+x)$ZnO–$(5+y)SiO_2$ glass system. Dilatometry testing reveals that substituting B_2O_3 with SiO_2 on a one-to-one molar basis enhances the T_g slightly from 374°C to 376°C and the T_d from 387°C to 392°C. Additionally, there's a minor decrease in the coefficient of thermal expansion, dropping from 10.2 ppm/°C to 10.0 ppm/°C. Such alterations are ascribed to the transition from the more flexible B–O bonds to the stronger and more rigid Si–O bonds, which enhances the strength and connectivity within the glass matrix. Conversely, when B_2O_3 is replaced with ZnO, there's a reduction in both T_g (dropping from 374°C to 345°C) and T_d (from 387°C to 364°C), and a rise in CTE (increasing from 10.2 to 10.7 ppm/°C). This effect stems from replacing the more resilient B–O bonds with the relatively less robust Zn–O bonds, which weakens the overall glass structure. Notably, the CTE values for glasses typically employed as sealants in Solid Oxide Fuel Cells range between 9–13 ppm/°C [38]. The CTE values for all studied glasses fall within this range, indicating their suitability as sealants in SOFC applications.

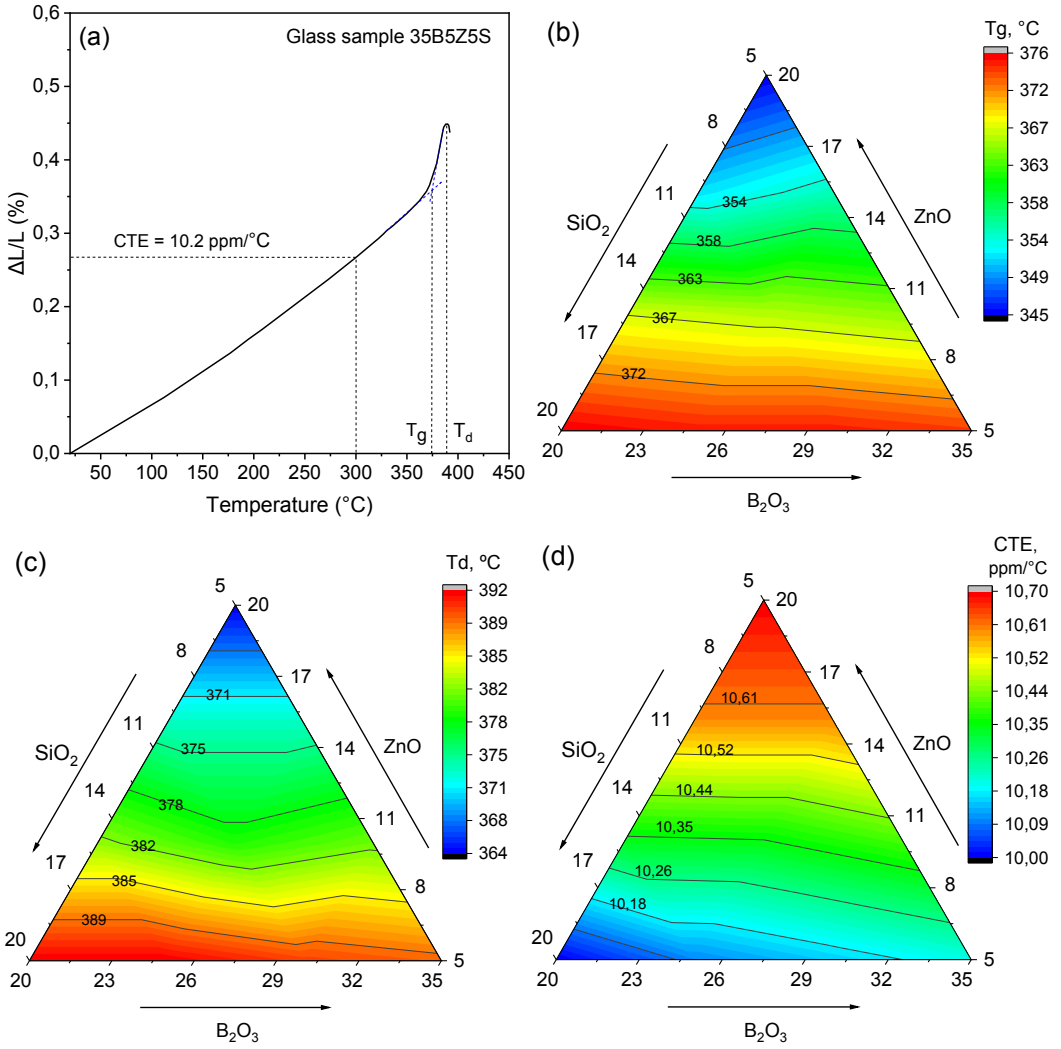

Fig. 6. Dilatometry curve for 35B5Z5S sample (a), with ternary plots showing the variation of T_g (b), T_d (c), and CTE (d) across compositions in the $55Bi_2O_3$–$(35-x-y)B_2O_3$–$(5+x)ZnO$–$(5+y)SiO_2$ system.

The study also highlights the impact of compositional changes on the glass's density, which increases from 7.264 to 7.333 g/cm^3 with the replacement of B_2O_3 by SiO_2, and from 7.264 to 7.565 g/cm^3 when substituted by ZnO, reflecting the additive nature of the oxides' densities involved, in ascending order: B_2O_3 (2.46 g/cm^3), SiO_2 (2.65 g/cm^3), and ZnO (5.61 g/cm^3). Table 2 shows that the molar volume behaves inversely to density, decreasing with the equimolar substitution of B_2O_3 by ZnO and SiO_2, which is attributed to the reduction of bond lengths or the tightening of the interatomic spacing within the glass network [39], leading to a more compact structure.

4. Conclusions

An enhanced and expanded series of bismuth borate glasses was developed, adhering to the formula $55Bi_2O_3$–$(35-x-y)B_2O_3$–$(5+x)ZnO$–$(5+y)SiO_2$, with varying concentrations of ZnO and SiO_2 ($0 \leq x, y \leq 15$ mol%). These novel glass materials were fabricated employing the traditional melt-quenching-annealing approach and were comprehensively analyzed using a suite of characterization methods such as XRD, SEM, FT-IR, DTA and dilatometry. The XRD and DTA assessments affirmed the glasses' amorphous structure, affirming their absence of crystalline long-

range order. The FTIR analysis revealed the presence of various structural units like BO_4, BO_3, BiO_6, BiO_3, ZnO_4, and SiO_4 within the investigated glass system.

The thermal behavior and stability of the glasses were determined through DTA and dilatometry, highlighting the influence of substituting B_2O_3 with ZnO and SiO_2 on the glass properties. Specifically, the substitution resulted in enhanced glass stability, with the $55Bi_2O_3$–$20B_2O_3$–20ZnO–$5SiO_2$ composition demonstrating the highest thermal stability (ΔT = 99°C). In this glass series, replacing B_2O_3 with SiO_2 strengthens the glass network, increasing T_g and T_d while decreasing CTE. Conversely, substituting B_2O_3 with ZnO weakens the network structure, leading to lower T_g and T_d and a higher CTE. The observed variations in density and molar volume across the glass series align with the anticipated effects based on the intrinsic properties of the constituent oxides.

Acknowledgements

The authors gratefully acknowledge the financial support the Ministry of Education and Science of Ukraine provided under Project No. 0123U102006.

References

[1] T. Maeder, Int. Mater. Rev. **58**, 3 (2013); https://doi.org/10.1179/1743280412Y.0000000010
[2] I. Dyamant, D. Itzhak, J. Hormadaly, J. Non Cryst. Solids. **351**, 3503 (2005); https://doi.org/10.1016/j.jnoncrysol.2005.08.031
[3] Y. Liu, B. Li, X. Shu, Z. Zhang, G. Wei, Y. Liu, S. Chen, Y. Xie, X. Lu, J. Hazard. Mater. **403**, 123588 (2021); https://doi.org/10.1016/j.jhazmat.2020.123588
[4] H. A. Saudi, H. A. Sallam, K. Abdullah, Phys. Mater. Chem. **2**(1), 20 (2014).
[5] H. Akhdar, Appl. Sci. **13**(16), 9332 (2023); https://doi.org/10.3390/app13169332
[6] S. P. Singh, B. Karmakar, Mater. Charact. **62**, 626 (2011); https://doi.org/10.1016/j.matchar.2011.04.007
[7] K. Biswas, A. D. Sontakke, R. Sen, K. Annapurna, Spectrochim. Acta A Mol. Biomol. Spectrosc. **112**, 301 (2013); https://doi.org/10.1016/j.saa.2013.04.062
[8] E. V. Karasik, Yu. S. Hordieiev, Voprosy Khimii i Khimicheskoi Tekhnologii **6**, 69 (2020); https://doi.org/10.32434/0321-4095-2020-133-6-69-74
[9] V. I. Goleus, Y. S. Hordieiev, A. V. Nosenko, Voprosy Khimii i Khimicheskoi Tekhnologii **4**, 92 (2018).
[10] A. N. D'Souza, N. S. Prabhu, K. Sharmila, M. I. Sayyed, H. M. Somshekarappa, G. Lakshminarayana, S. Mandal, S. D. Kamath, J. Non Cryst. Solids. **542**, 120136 (2020); https://doi.org/10.1016/j.jnoncrysol.2020.120136
[11] N. Sugimoto, J. Am. Ceram. Soc. **85**, 1083 (2002); https://doi.org/10.1111/j.1151-2916.2002.tb00226.x
[12] C. Fredericci, H. N. Yoshimura, A. L. Molisani, H. Fellegara, J. Non Cryst. Solids. **354**, 4777 (2008); https://doi.org/10.1016/j.jnoncrysol.2008.04.026
[13] Y. Gao, J.-J. Ma, Y. Chen, M.-H. Wang, J. Mater. Sci.: Mater. Electron. **34**, 693 (2023); https://doi.org/10.1007/s10854-023-10096-4
[14] Yu. S. Hordieiev, A. V. Zaichuk, Journal of Ovonic Research **19**, 471 (2023); https://doi.org/10.15251/jor.2023.194.471
[15] Yu. S. Hordieiev, A. V. Zaichuk, Chalcogenide Lett. **21**, 243 (2024); https://doi.org/10.15251/CL.2024.213.243
[16] Y. Hordieiev, A. Zaichuk, MRS Advances (2024); https://doi.org/10.1557/s43580-024-00820-5
[17] Y. B. Saddeek, Philos. Mag. (Abingdon). **89**, 2305 (2009); https://doi.org/10.1080/14786430903070936
[18] Y. S. Hordieiev, A. V. Zaichuk, Results in Materials. **19**, 100442 (2023); https://doi.org/10.1016/j.rinma.2023.100442

[19] Yu. S. Hordieiev, A. V. Zaichuk, J. Inorg. Organomet. Polym. Mater. **33**(2), 591 (2023); https://doi.org/10.1007/s10904-022-02526-3
[20] A. Kaur, A. Khanna, H. Bhatt, M. Gónzález-Barriuso, F. González, B. Chen, M. N. Deo, J. Non Cryst. Solids. **470**, 19 (2017); https://doi.org/10.1016/j.jnoncrysol.2017.04.028
[21] Y. B. Saddeek, K. Aly, G. Abbady, N. Afify, K. H. S. Shaaban, A. Dahshan, J. Non Cryst. Solids. **454**, 13 (2016); http://doi.org/10.1016/j.jnoncrysol.2016.10.023
[22] I. Ardelean, S. Cora, D. Rusu, Physica B Condens. Matter. **403**, 3682 (2008); https://doi.org/10.1016/j.physb.2008.06.016
[23] R. Iordanova, M. Milanova, L. Aleksandrov, A. Khanna, J. Non Cryst. Solids. **481**, 254 (2018); https://doi.org/10.1016/j.jnoncrysol.2017.10.041
[24] L. Xia, L. Wang, Q. Xiao, Z. Li, W. You, Q. Zhang, J. Non Cryst. Solids. **476**, 151 (2017); https://doi.org/10.1016/j.jnoncrysol.2017.09.049
[25] A. Abd El-Moneim, M. A. Azooz, H. A. Hashem, A. M. Fayad, R. L. Elwan, Sci. Rep. **13**, 12788 (2023); https://doi.org/10.1038/s41598-023-39489-5
[26] Yu. S. Hordieiev, A. V. Zaichuk, Chalcogenide Letters **19**(12), 891 (2022); https://doi.org/10.15251/CL.2022.1912.891
[27] D. Nain, D. Maan, J. Ahlawat, Meenakshi, Silicon (2023); https://doi.org/10.1007/s12633-023-02832-6
[28] M. Lesniak, J. Zmojda, M. Kochanowicz, P. Miluski, A. Baranowska, G. Mach, M. Kuwik, J. Pisarska, W. A. Pisarski, D. Dorosz, Materials **12**, 3429 (2019); https://doi.org/10.3390/ma12203429
[29] V. Dimitrov, T. Komatsu, J. Chemi. Technol. Metall. **45**(3), 219 (2010).
[30] K. Ariane, A. Tamayo, A. Chorfa, F. Rubio, J. Rubio, Bol. Soc. Esp. Ceram. Vidr. **59**, 239 (2020); https://doi.org/10.1016/j.bsecv.2019.11.003
[31] J. E. Shelby, Introduction to Glass Science and Technology, The Royal Society of Chemistry, London, (2020); https://doi.org/10.1039/9781839169229
[32] A. Dietzel, Glasstech Ber. **22**, 41 (1968).
[33] M. Saad, M. Poulain, Mater. Sci. For. **19–20**, 11 (1987); https://doi.org/10.4028/www.scientific.net/msf.19-20.11
[34] A. Hrubý, Czechoslov. J. Phys. **22**, 1187 (1972); https://doi.org/10.1007/bf01690134
[35] M. D. Dolan, N. C. Dave, A. Y. Ilyushechkin, L. D. Morpeth, K. G. McLennan, J. Memb. Sci. **285**, 30 (2006); https://doi.org/10.1016/j.memsci.2006.09.014
[36] W. Kauzmann, Chem. Rev. **43**, 219 (1948); https://doi.org/10.1021/cr60135a002
[37] A. V. Nosenko, Y. S. Hordieiev, V. I. Goleus, Voprosy Khimii i Khimicheskoi Tekhnologii **1**, 87 (2018).
[38] K. L. Ley, M. Krumpelt, R. Kumar, J. H. Meiser, I. Bloom, J. Mater. Res. **11**, 1489 (1996); https://doi.org/10.1557/JMR.1996.0185
[39] Y. S. Hordieiev, A. V. Zaichuk, MRS Advances **8**, 201 (2023); https://doi.org/10.1557/s43580-023-00511-7